Engineering Analysis with Boundary Elements 189 (2026) 106822

Contents lists available at ScienceDirect

Engineering Analysis with Boundary Elements

journal homepage: www.elsevier.com/locate/enganabound

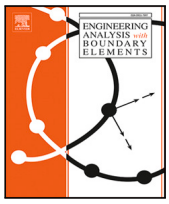

Integrated soil–structure model for seismic analysis of jacket-based offshore wind turbines☆

J.D.R. Bordón *, R. Quevedo-Reina, G.M. Álamo, C. Medina, L.A. Padrón, J.J. Aznárez, O. Maeso

Instituto Universitario de Sistemas Inteligentes y Aplicaciones Numéricas en Ingeniería (SIANI), Universidad de Las Palmas de Gran Canaria (ULPGC), Edificio Central del Parque Científico y Tecnológico, Campus Universitario de Tafira, Las Palmas de Gran Canaria, 35017, Las Palmas, Spain

ARTICLE INFO

Keywords:
BEM-FEM coupling
Offshore wind turbines
Jacket structures
Piles
Suction caissons
Seismic response

ABSTRACT

This paper presents a boundary element–finite element model for the seismic analysis of jacket-based Offshore Wind Turbines (OWTs). Unlike traditional substructuring methods that rely on simplified spring-based foundations, this study proposes an elastodynamic formulation in the frequency domain that treats the structure and the soil as a single coupled system. By using Green's functions for a layered viscoelastic half-space, this model captures the full spatial nature of seismic excitation and energy radiation without requiring soil mesh discretization. This direct approach provides an advanced and natural representation of Soil–Structure Interaction (SSI). A comparative study is performed to evaluate the response of OWTs using the proposed model against fixed base and simplified engineering SSI approaches. The study assesses three- and four-legged jackets at both 20 m and 50 m water depths, using pile and suction caisson foundations in homogeneous and non-homogeneous soils. The results quantify SSI effects such as the reduction of natural frequencies and the increase in system damping. Findings indicate that while simplified spring-dashpot models from existing literature are easy to incorporate, they can be unreliable for complex configurations. This emphasizes that a direct approach is essential for robust seismic design and analysis of multi-supported offshore wind structures.

1. Introduction

Offshore wind energy is one of the most promising and accessible sources of renewable energy in the short term [1]. Offshore wind farms have several significant advantages over onshore ones. From a technical point of view, wind resources at sea are of better quality, with higher wind speeds, fewer obstacles, and more stable wind direction. On the other hand, onshore installations have a significant impact on local communities and occupied areas, which are also limited in their availability. Thus, 8 GW of offshore wind energy was installed globally in 2024, giving a total installed operating capacity of over 83 GW [2]. Based on announced and developing projects, it is estimated that total installed capacity using this technology could reach around 190 GW by 2029 [2].

Despite the offshore wind industry's interest in floating technology and its evolution in recent years, most of the Offshore Wind Turbines (OWTs) currently being installed, and those to be installed in the coming years, will be fixed directly to the seabed [2]. The support structure used depends on the depth of the sea and the geotechnical properties of the site selected for installation. It can be reduced to a single vertical element connecting the wind turbine to the foundation, or it can be an arrangement of resistant elements with varying degrees of complexity (jacket, tripods), usually founded on piles or suction caissons (see e.g. [3,4]). In practice, most current offshore wind farms are installed in shallow waters (up to 30 m deep) and the turbines are mounted on monopiles. However, as more powerful wind turbines are installed at greater depths, the use of structures founded on multiple supports is becoming increasingly common. In fact, this technology is evolving in the development of structural designs that allow these devices to be installed at ever greater depths and, as a result, at greater distances from the coast. Thus, according to the data available to date, the deepest fixed-bottom OWT in operation is installed on a jacket-type substructure in waters 58.6 m deep at the Seagreen Project Wind Farm in Scotland, 27 km off the coast of Angus [2]. At present, everything indicates that improvements in design and construction techniques will allow for an expansion of the jacket foundation technique in the coming years.

When discussing the procedures and tools for analyzing and designing the support structure of OWTs, research has mainly focused on

☆ This article is part of a Special issue entitled: 'BEM Memory of Domínguez' published in Engineering Analysis with Boundary Elements.

* Corresponding author.
E-mail address: jacobdavid.rodriguezbordon@ulpgc.es (J.D.R. Bordón).

https://doi.org/10.1016/j.enganabound.2026.106822
Received 25 January 2026; Received in revised form 31 March 2026; Accepted 13 May 2026
Available online 22 May 2026

aerodynamic and hydrodynamic subjects, while the study of structural response to seismic loads has been less addressed in the literature. However, for some time now, certain aspects of this problem have begun to attract the attention of analysts: (1) the growing demand for clean energy and the limited availability of suitable non-seismic sites not already exploited are driving the expansion of this technology into seismically active regions in East Asia, Europe, and North America, where experience in this regard can be considered limited, and (2) the increasing size of new wind turbines may lead to significant variations in their responses or in the safety factors of their support structures, as well as an increase in the potential impact of their collapse. In this regard, the nominal power of OWT purchase orders in Europe in 2024 was already 14.8 MW [5].

There is abundant literature showing that OWTs, due to their size and structural morphology, are dynamically sensitive systems in which Soil–Structure Interaction (SSI) effects have a decisive influence on their behavior. These interaction phenomena between the soil and the structure depend on the properties of both and can modify the natural frequency and damping of the system and, with this, its overall response to dynamic loads. These are, therefore, effects that cannot be ignored and have been considered in different ways and with varying degrees of accuracy, depending on the objective pursued, in many of the models developed for the analysis of this type of structure [4].

The characteristics, performance, complexity and scope of existing SSI models vary greatly and, in a very basic classification, depend mainly on whether or not the seabed behavior is considered linear, taking into account the problem to be addressed. Non-linear approaches frequently use Winkler-type models that idealize soil–foundation interaction through decoupled springs, usually known as $p-y$ curves for lateral response (common in monopiles), or $t-z$ and $q-z$ curves when axial response is the primary concern, as is typical for jacket foundations. However, for more complex nonlinear effects such as soil fracture or advanced constitutive behavior, continuous medium models employing the Finite Element Method (FEM) are typically preferred. Models that assume linear soil behavior also allow for formulation in the frequency domain and, depending on the problem, it is common to use substructure techniques, usually through impedance functions that concentrate the response of the soil–foundation assembly that can even be integrated into other available analysis codes. However, it is also interesting to address direct formulations that allow for a coupled analysis of all the regions (super-structures, foundations, soils) involved in the problem. This approach has several advantages, such as the rigor in considering the geometry of each foundation, their flexibility, the filtering of incoming waves, and the interaction effects in multi-supported configurations. These elastodynamic models for SSI, in their most advanced version, have historically been developed using boundary integral formulations that have made it possible to deal with some specific aspects of the problem in a very natural way, such as the geometry of the half-space, the inherent condition of energy radiation to infinity, or the spatial nature of the excitation and seismic response along the soil–foundation interface, all of this even in the case of non-homogeneous soils. In the numerical treatment of this type of SSI approach, the pioneering work of Professor Domínguez at MIT [6,7] using the "new" Boundary Element Method (BEM) and his subsequent advances with some of his collaborators [8–14] must be highlighted. The result of all this work has been the development of integrated dynamic models of increasing complexity that have been applied to a multitude of problems related to the dynamic characterization of structures or their seismic response, including, more recently, the problem that concerns us now in the case of OWTs (see e.g. [15,16]).

Thus, the aim of this paper is to extend these direct elastodynamic models to the problem of OWTs on jacket substructures subjected to seismic loading. We therefore present a dynamic model that integrates all the elements of the system into a coupled analysis: wind turbine, jacket, foundation (suction caissons or piles) and stratified seabed with a vertical incident field of shear waves to simulate the seismic excitation. The wind turbine and jacket are modeled using Timoshenko beam finite elements connected through rigid joints, and added masses for the rotor-nacelle-assembly and transition piece. The water–structure interaction between the sea water and the jacket is included via added masses [17]. Each foundation is rigidly connected to the jacket and they can be modeled via beam finite elements or shell finite elements representing either piles or suction caissons depending on their length to diameter ratio. The SSI between these foundations and the surrounding soil is included via a boundary element formulation based on a Green's function for a horizontally layered viscoelastic half-space [18]. The formulation considered in this paper generalizes previous works [19–21] and it incorporates soil–beam and soil–shell interaction in stratified soils without actually needing to discretize any other part of the soil.

While the wind turbine itself is not difficult to define from manufacturer data, the definition of the jacket and foundation requires establishing many topological and geometrical parameters which are site-specific. In order to reduce the number of input data to only site conditions (wind, sea, and soil characterization), wind turbine, type of jacket and foundation (three- or four-legged jacket on suction caissons or piles with specified dimensions), an auxiliary semi-automated jacket preliminary design procedure has also been used [22]. Although the dynamic model is independent of this auxiliary procedure, it facilitates a more direct and realistic analysis of the relationship between system dynamics and site-specific conditions.

The rest of the paper is organized as follows: Section 2 describes the problem and the proposed integrated soil–structure model. Section 3 uses this model to study the effects of SSI on the seismic response of a practical OWT application (i.e. displacements, shear, axial forces, and bending moments), considering different jackets, foundations and soils, and using more simplified models for reference. Finally, Section 4 presents the paper's main conclusions and suggests topics for further research.

2. Methodology

In this section, the proposed model is described in detail. Fig. 1 depicts the physical system under consideration, where the wind turbine is supported by a partially submerged three- or four-legged jacket structure founded on suction caissons or piles installed in a stratified soil.

The model assumes linear elastic and small displacements behavior. It is formulated in the frequency-domain ω, where $\omega = 2\pi f$ is the angular frequency (rad s^{-1}) and f is the frequency in (s^{-1} = Hz). For the sake of brevity, the time factor $e^{i\omega t}$ accompanying complex time-harmonic variables is omitted by default ($i = \sqrt{-1}$ is the imaginary unit).

Since the focus is put on assessing SSI phenomena, particularly on its effects on the foundation and main structural members (jacket and tower), the rotor is considered perfectly balanced and the interaction between blades and the rest of the system is neglected. Therefore, the rotor (hub and blades) are reduced to a lumped mass matrix at the tower top. In a broader picture, this is called a Linear Time-Invariant (LTI) system. A fully rigorous analysis would require considering not only the blade elements, which could also be done with the present model, but also the rotation of hub and blades at a given speed, which results in what is called a Linear Periodically Time-Varying (LPTV) system [23–25]. This type of system can be studied through a more costly time-domain analysis or Floquet modal analysis. The LTI approach considered in this paper is also used in most of the literature regarding SSI because it is able to capture most of the relevant physical phenomena at a reasonable computational cost.

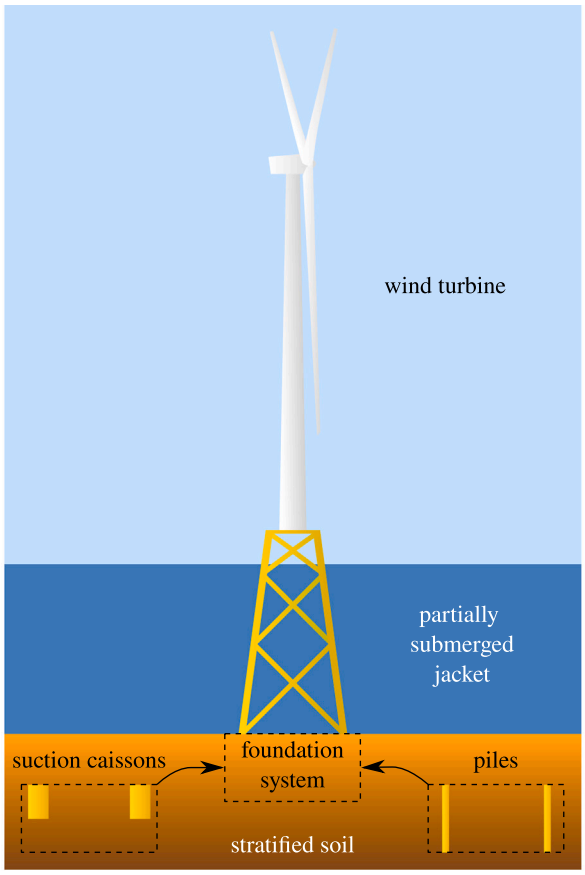

Fig. 1. Jacket-based Offshore Wind Turbine.

2.1. Structure

A jacket-based OWT is a complex system, but from the structural point of view, the following main parts can be identified: the rotor-nacelle assembly, turbine tower, transition piece, jacket, jacket-foundation connection, and foundation. In the present work, these parts are entirely modeled using shear-deformable and locking-free finite elements, i.e. Timoshenko beam finite elements [26] and Reissner–Mindlin shell finite elements [27], and structural inertia, added mass, and damping. The shear correction factor for the Timoshenko beam elements is taken from [28], while in the case of shell elements the usual 5/6 factor is considered. The primary features and properties of the models used for each part of the system are detailed in the following subsections.

2.1.1. Rotor-Nacelle assembly

The Rotor-Nacelle Assembly (RNA) comprises the blades, hub, shaft, the electromechanical system inside the nacelle, the nacelle itself, and the bearing. This assembly is a complex electromechanical system relevant for the operation of the wind turbine. However, for the purpose of general structural dynamic characterization and seismic analysis, it can be reduced to a lumped mass matrix at the tower top (see Fig. 2). In a recent research [29], the influence of RNA modeling has been addressed. It concluded that the type of modeling considered here is appropriate, although conservative in the upper part of the tower regarding maximum stresses. Depending on the available data from the manufacturer or other sources, and the type of analysis, this mass matrix can be formulated with different levels of rigor and completeness. The nodal degrees of freedom at tower top are its displacements and rotations: $\mathbf{a}^{(\mathrm{tt})} = (u_x, u_y, u_z, \theta_x, \theta_y, \theta_z)^{\mathrm{T}}$. Assuming complete availability of data allows to reduce the RNA mass to the tower top node in the following way:

$$\mathbf{M}_{\mathrm{RNA}} = \begin{bmatrix} \mathbf{M}_{\mathrm{RNA},0} & \mathbf{M}_{\mathrm{RNA},1} \\ \mathbf{M}_{\mathrm{RNA},1}^{T} & \mathbf{M}_{\mathrm{RNA},2} \end{bmatrix} \tag{1}$$

where $\mathbf{M}_{\mathrm{RNA},0}$, $\mathbf{M}_{\mathrm{RNA},1}$ and $\mathbf{M}_{\mathrm{RNA},2}$ are respectively the standard 3×3 matrices containing the zero-, first- and second-order moments of mass. The most important contribution is that of the mass submatrix $\mathbf{M}_{\mathrm{RNA},0}$:

$$\mathbf{M}_{\mathrm{RNA},0} = m_{\mathrm{RNA}} \mathbf{I}_{3\times 3} \tag{2}$$

which is a diagonal matrix containing the total mass of the RNA and thus all the translational inertia. The RNA total mass can be further decomposed as:

$$m_{\mathrm{RNA}} = 3m_{\mathrm{blade}} + m_{\mathrm{hub}} + m_{\mathrm{nacelle}} + m_{\mathrm{bearing}} = m_{\mathrm{rotor}} + m_{\mathrm{nacelle}} + m_{\mathrm{bearing}} \tag{3}$$

where m_{nacelle} contains all the mass of the nacelle and the equipment contained in it. Second in importance is the mass submatrix $\mathbf{M}_{\mathrm{RNA},2}$:

$$\mathbf{M}_{\mathrm{RNA},2} = \begin{bmatrix} I_{\mathrm{roll}} & 0 & I_{x'z'} \\ 0 & I_{\mathrm{pitch}-y'} & 0 \\ I_{x'z'} & 0 & I_{\mathrm{yaw}-z'} \end{bmatrix} \tag{4}$$

which is a matrix containing the moments of inertia, i.e. all the RNA rotational inertia, with respect to the x', y', and z' axes located at the tower top. Here, it is assumed that the x' axis located at the tower top is parallel to the rotor axis x'' and the global x axis, and z' located at the tower top and z'' located at the hub are parallel to the global z axis. Due to the RNA mass symmetry with respect to the $x'z'$ plane, products of inertia $I_{x'y'}$ and $I_{y'z'}$ are null, and the product of inertia I_{xz}, although not null, is typically small when compared to the diagonal terms. Finally, the mass submatrix $\mathbf{M}_{\mathrm{RNA},1}$ appears as a consequence of the RNA mass center not being coincident with the tower top:

$$\mathbf{M}_{\mathrm{RNA},1} = \begin{bmatrix} 0 & -M_z & 0 \\ M_z & 0 & M_x \\ 0 & -M_x & 0 \end{bmatrix} \tag{5}$$

where:

$$M_x = m_{\mathrm{rotor}}(x_{\mathrm{rotor}} - x_{\mathrm{tower-top}}) + m_{\mathrm{nacelle}}(x_{\mathrm{nacelle}} - x_{\mathrm{tower-top}}) \tag{6}$$

$$M_z = m_{\mathrm{rotor}}(z_{\mathrm{rotor}} - z_{\mathrm{tower-top}}) + m_{\mathrm{nacelle}}(z_{\mathrm{nacelle}} - z_{\mathrm{tower-top}}) \tag{7}$$

producing a coupling between translations and rotations of the tower top. Again, because the mass center is contained in the $x'z'$ plane, i.e. $y_{\mathrm{rotor}} = y_{\mathrm{nacelle}} = 0$, there is only a partial coupling.

2.1.2. Turbine tower

The turbine tower is a steel tower composed by many cylindrical shell sections with varying diameter and shell thickness. It starts at the tower bottom, coincident with the jacket top and the transition piece plate, with a diameter $D_{\mathrm{tower-bottom}}$ and thickness $t_{\mathrm{tower-bottom}}$, and reaches the tower top with a diameter $D_{\mathrm{tower-top}}$ and thickness $t_{\mathrm{tower-top}}$, having a total height of h_{tower}. If available, each tower section j can be defined through its own height $h_{\mathrm{tower},j}$, diameter $D_{\mathrm{tower},j}$ and thickness $t_{\mathrm{tower},j}$, otherwise an interpolated diameter and thickness are taken from the top and bottom ones. Given the typical frequency range for global dynamic and seismic analyses (up to 10 or 20 Hz), the tower can be modeled as Timoshenko beam elements.

2.1.3. Transition piece

The transition piece is a complex multiple joint connection between the tower and the jacket. There are many topologies considered in the literature and in practice. In its own right, it has been subjected to considerable research, see e.g. [30]. Here, a simple design is considered, where a triangular (for three-legged jackets) or square (for four-legged jackets) plate is welded to the legs at the jacket top and to the tower bottom, see Fig. 3. For simplicity, the plate has a constant

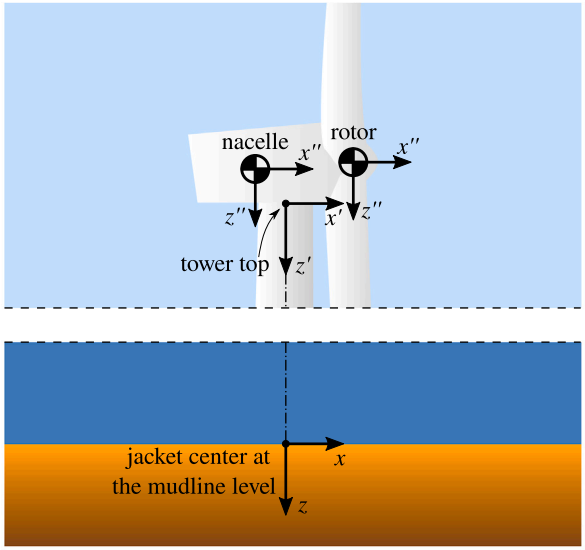

Fig. 2. Rotor-Nacelle-Assembly idealization.

thickness, which in the present paper is taken as 0.2 m. Diagonal members connect each leg at the jacket top to the tower at a height equal to the leg spacing at the top. These members have cross-sections similar to those of the legs. This transition piece design is not intended to be completely realistic, but it provides a rigid connection between jacket and tower and a mass of the same order of magnitude to that encountered in practice.

2.1.4. Jacket

Jackets are partially submerged lattice structures composed by tubular members that transfer loads from the base of the wind turbine tower to the foundation system. They are subjected to complex loading which depends on the wind turbine and many environmental factors (wind, water depth, waves and current, soil, and others). With all this information and the requirements from the wind turbine manufacturer, client, guidelines and/or regulations, the design of a jacket becomes quite complex. Many structural topologies have been proposed, and there is plenty of research and tools devoted to jacket design [32]. In order to size the jackets to be used in this study, a basic automated design framework developed by some of the authors according to DNV and IEC codes was used [22].

2.1.5. Jacket-foundation connection

The connection of the jacket to the foundations is a very important part of the system since it transfers all loads to the foundation system. Here, it is performed at the lowest jacket joints, and thus each joint rigidly connects the leg, two bracing members and the foundation.

2.1.6. Foundation

Two types of foundations are considered: suction caissons and piles. Piles used in OWTs are steel hollow circular piles, and thus both suction caissons and piles are topologically similar. The only difference lies on the length to diameter (L/D) and thickness to diameter (t/D) ratios, which in the case of piles are higher ($L/D > 5$, $t/D \sim 0.01$) that in the case of suction caissons ($L/D < 6$, $t/D \sim 0.001$). The lid of the suction caisson is considered to be rigid.

From the modeling point of view, it is quite clear that piles can be modeled with beam elements and short suction caissons have to be modeled with shell elements (see Fig. 4). However, there is a range of length to diameter ratios ($2 < L/D < 6$) where it is questionable which type of modeling is more appropriate. From the computational cost point of view, it is always preferable to use a beam-like model, even if the foundation is a suction caisson, because the more rigorous shell model is computationally costlier. This is due to the soil–structure boundary element/finite element coupled model, and in particular from the boundary element side (Green's function evaluation), which is described in Section 2.3.2. To this end, a comprehensive study was performed in [33], concluding that the validity of the beam model can reach down to $L/D > 2$ depending on the range of frequencies to be considered. In this study, piles are modeled with beam elements and suction caissons with shell elements.

2.2. Air and water Fluid–Structure Interaction

The OWT is in contact with air and water, and thus there are Fluid–Structure Interaction (FSI) phenomena taking place. Since linear elastic and small amplitude vibrations are assumed, this interaction can only be considered as acoustic phenomena or as additional mass and damping.

The air–structure interaction is particularly difficult to assess with a frequency-domain model. This phenomena mainly introduces additional damping through the blades, which depends on the wind and rotor speeds [34]. Although there are ways of considering it via additional dampers, no aerodynamic damping is considered here since its influence in the low frequency response of OWT is usually small when compared to other factors.

On the other hand, water–structure interaction is quite relevant, particularly for frequencies beyond the fundamental one, see e.g. [35]. Furthermore, the effects on the structure are relatively easy to introduce. There are two sources of interaction: (1) the confined water inside submerged members, and (2) the induced motion of the fluid due to the lateral motion of the member. The first source of interaction is easily introduced by adding the water translational inertia to the beam element mass matrix, i.e. an added mass per unit length of $\rho_{\text{water}}\pi(D^{(e)}-2t^{(e)})^2/4$, where $D^{(e)}$ and $t^{(e)}$ are the outer diameter and thickness of element. The second source of interaction can also be described in terms of added mass and damping [17], although damping is generally negligible. This added mass is also introduced in the element mass matrix, but only for the lateral translational inertia. For submerged tubular members, the added mass per unit length is simply the product of the water density by the external area of the member, i.e. $\rho_{\text{water}}\pi\left(D^{(e)}\right)^2/4$. This simple approach is effective and is used in practice, but ignores the structure real geometry since it is obtained from assuming infinitely long and isolated members interacting with the surrounding fluid.

2.3. Soil and Soil–Structure Interaction

The soil in which the OWT is founded is considered as a horizontally stratified elastic half-space, where each horizontal layer is homogeneous and isotropic. Each layer j of the N_{layers} is defined by the properties: density $\rho_{\text{soil},j}$, shear modulus $\mu_{\text{soil},j}$, Poisson's ratio $\nu_{\text{soil},j}$, and hysteretic damping $\xi_{\text{soil},j}$. As usual, hysteretic damping is introduced via complex shear modulus $\mu_{\text{soil},j} = \text{Re}\left[\mu_{\text{soil},j}\right]\cdot\left(1+\text{i}2\xi_{\text{soil},j}\right)$. The soil that can be modeled is thus a quite general one.

The Soil–Structure Interaction is introduced via a rigorous coupled boundary element–finite element model which generalizes previous models for piles and suction caissons [19–21]. The proposed coupled model allows considering beams and/or shells buried in a stratified soil. It is a development of an earlier version of MultiFEBE [36], which incorporates BEM formulations that can only deal with regions of homogeneous nature. In the next sections, this model is described.

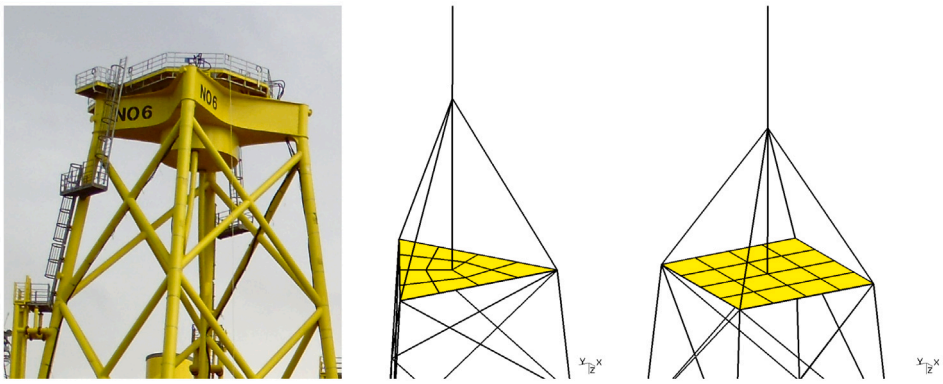

(a) Real picture adapted from [31] (public domain image).

(b) Modeling for three- and four-legged jackets

Fig. 3. Transition piece modeling.

2.3.1. Finite element formulation

From the finite element point of view, the already mentioned Timoshenko beam finite elements [26] and Reissner–Mindlin shell finite elements [27] are used for modeling the foundation. The usual element equilibrium equation for time harmonic analyses can be written in matrix form as:

$$\left(\mathbf{K}^{(e)} - \omega^2 \mathbf{M}^{(e)}\right) \mathbf{a}^{(e)} - \mathbf{Q}^{(e)} \mathbf{f}^{(e)} = \mathbf{q}^{(e)} \tag{8}$$

where $\mathbf{K}^{(e)}$ and $\mathbf{M}^{(e)}$ respectively are the element stiffness and mass matrices, $\mathbf{a}^{(e)}$ is the vector of element degrees of freedom, $\mathbf{Q}^{(e)}$ is the matrix which transforms mid-line or mid-surface distributed forces $\mathbf{f}^{(e)}$ into equivalent nodal loads, and $\mathbf{q}^{(e)}$ is the element equilibrating loads vector. More specifically, for an element e with N nodes:

$$\mathbf{a}^{(e)} = \left(\mathbf{a}_1^{(e)}, \ldots, \mathbf{a}_N^{(e)}\right)^T = \left(\mathbf{a}^{(n_1)}, \ldots, \mathbf{a}^{(n_N)}\right)^T \tag{9}$$

$$\mathbf{f}^{(e)} = \left(\mathbf{f}_1^{(e)}, \ldots, \mathbf{f}_N^{(e)}\right)^T = \left(\mathbf{f}^{(n_1)}, \ldots, \mathbf{f}^{(n_N)}\right)^T \tag{10}$$

and, for a given node n:

$$\mathbf{a}^{(n)} = \left(u_x^{(n)}, u_y^{(n)}, u_z^{(n)}, \theta_x^{(n)}, \theta_y^{(n)}, \theta_z^{(n)}\right)^T \quad \text{(6 DOF beam or shell node)} \tag{11}$$

$$\mathbf{a}^{(n)} = \left(u_x^{(n)}, u_y^{(n)}, u_z^{(n)}, \alpha^{(n)}, \beta^{(n)}\right)^T \quad \text{(5 DOF shell node with local rotations)} \tag{12}$$

$$\mathbf{f}^{(n)} = \left(f_x^{(n)}, f_y^{(n)}, f_z^{(n)}\right)^T \quad \text{(beam: forces per unit length; shell: forces per unit surface)} \tag{13}$$

It is often the case that distributed forces $\mathbf{f}^{(e)}$ are prescribed, but in the present model they remain as active degrees of freedom.

2.3.2. Boundary element formulation

The starting point of the Boundary Element Method [37] is the boundary integral equation:

$$c_{lk}^{\mathrm{i}} u_k^{\mathrm{i}} + \int_\Gamma t_{lk}^* u_k \, \mathrm{d}\Gamma = \int_\Gamma u_{lk}^* t_k \, \mathrm{d}\Gamma + \int_\Omega u_{lk}^* b_k \, \mathrm{d}\Omega, \quad l,k = 1,2,3 \equiv x,y,z \tag{14}$$

where Einstein summation is implied, and c_{lk}^{i} is the so-called free-term [38]. It relates body loads b_k throughout the domain Ω, displacements u_k and tractions $t_k = \sigma_{kj} n_j$ throughout the boundary $\Gamma = \partial\Omega$, and the displacement u_k^{i} at the collocation point of the point load. The main ingredient which makes this relation possible is the Green's function in terms of displacements u_{lk}^* and tractions $t_{lk}^* = \sigma_{lkj}^* n_j$, where the first index l is related to the load direction, the second index k is related to the observation direction, and n_j is the outward unit normal at the observation point ($j = 1,2,3$ is a dummy index). In this work, a Green's function for a horizontally layered elastic half-space is used [18]. Because the considered Green's function already fulfills the traction-free conditions at the free-surface and the stratigraphy, integrals along Γ are null except where these conditions are broken. Therefore, boundary elements are only needed at suction caisson lids, but given the traction-free condition at the free surface, the corresponding integral including t_{lk}^* is null. While body loads are typically treated as prescribed data, the present model employs them as active degrees of freedom to represent soil–structure interaction for buried beams and shells via line or surface loads. This way, the boundary integral equation can be written as:

$$c_{lk}^{\mathrm{i}} u_k^{\mathrm{i}} = \int_{\Gamma_{\mathrm{lids}}} u_{lk}^* t_k \, \mathrm{d}\Gamma + \int_{\Upsilon_{\mathrm{beams}}} u_{lk}^* b_k \, \mathrm{d}\Upsilon + \int_{\Pi_{\mathrm{shells}}} u_{lk}^* b_k \, \mathrm{d}\Pi \tag{15}$$

where Γ_{lids} represents the suction caisson lids, $\Upsilon_{\mathrm{beams}}$ represents the line loads b_k along beams mid-line, and Π_{shells} represents the surface loads b_k throughout shells mid-surface.

The discretization of the previous equation follows the usual procedure [37]. Two-dimensional isoparametric Lagrange elements are used for the lids surface Γ_{lids} (boundary elements). Also, two-dimensional isoparametric Lagrange elements are used for the shells mid-surface Π_{shells} (surface load elements). One-dimensional isoparametric Lagrange elements are used for the beams mid-line $\Upsilon_{\mathrm{beams}}$ (line load elements). For a given boundary element node n, displacements and tractions can be written as:

$$\mathbf{u}^{(n)} = \left(u_x^{(n)}, u_y^{(n)}, u_z^{(n)}\right)^T, \ \mathbf{t}^{(n)} = \left(t_x^{(n)}, t_y^{(n)}, t_z^{(n)}\right)^T \tag{16}$$

For a given line or surface load element node n, displacements and body loads can be written as:

$$\mathbf{u}^{(n)} = \left(u_x^{(n)}, u_y^{(n)}, u_z^{(n)}\right)^T, \ \mathbf{b}^{(n)} = \left(b_x^{(n)}, b_y^{(n)}, b_z^{(n)}\right)^T \tag{17}$$

The collocation procedure is the conventional one for the boundary and surface load elements, where nodal collocation is performed at all nodes except at nodes located along the boundary of the surface, see e.g. [21]. For line load elements, a non-nodal collocation procedure is required, see [19].

The evaluation of the considered Green's function is computationally expensive. Taking into account that the number of Green's function evaluations is proportional to the square number of nodes of the boundary element discretization and the number of Gauss points in the numerical integration scheme, the implementation efficiency is crucial. In order to keep the computational costs as low as possible, an appropriate database storing each new evaluation is used. Apart from the stratigraphy and the frequency, this Green's function can be formulated such that it depends on the source depth s, observation point depth z, and the radial distance r between source and observation point.

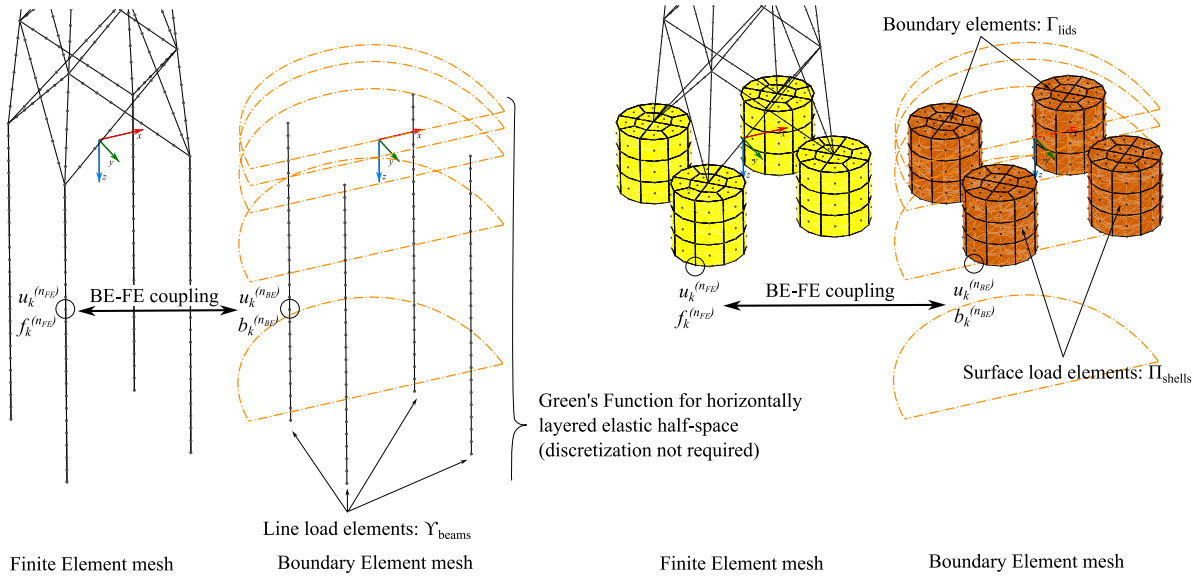

Fig. 4. Exploded view of the Soil and Soil–Structure Interaction modeling approach for piles (left) and suction caissons (right). Example of a four-legged jacket discretized with quadratic elements.

Therefore, any evaluation request sharing the same (s, z, r) coordinates can be retrieved from the database at a much lower computational cost. In order to take advantage of this, the mesh must be as regular as possible. As seen in Fig. 4, the regularity is very easy to achieve for line load elements (beam–soil interaction) by simply having the same discretization for all the foundations. On the other hand, for the case of surface load elements (shell–soil interaction) not only each foundation should have the same discretization, but each foundation mesh should have as much self-repetition as possible, as illustrated in Fig. 4.

2.3.3. Boundary element–finite element coupling

Assuming a conforming mesh between boundary or body load elements and finite elements, a direct coupling between both can be performed. This means that a node-by-node coupling can be applied. The coupling equations assumes welded contact conditions via displacement compatibility and equilibrium at the interface:

- For a boundary element node n_{BE} coincident with a finite element node n_{FE}:

$$u_k^{(n_{\mathrm{FE}})} = u_k^{(n_{\mathrm{BE}})}, \quad f_k^{(n_{\mathrm{FE}})} + t_k^{(n_{\mathrm{BE}})} = 0 \tag{18}$$

  where $k = 1, 2, 3 \equiv x, y, z$. Then $u_k^{(n_{\mathrm{FE}})}$ and $t_k^{(n_{\mathrm{BE}})}$ remain as the active degrees of freedom in the linear system of equations. In the present paper, these are applied to the elements discretizing the suction caisson lid.
- For a body (line or surface) load element node n_{LE} coincident with a finite element node n_{FE}:

$$u_k^{(n_{\mathrm{FE}})} = u_k^{(n_{\mathrm{LE}})}, \quad f_k^{(n_{\mathrm{FE}})} + b_k^{(n_{\mathrm{LE}})} = 0 \tag{19}$$

  and then $u_k^{(n_{\mathrm{FE}})}$ and $b_k^{(n_{\mathrm{LE}})}$ remain as the active degrees of freedom in the linear system of equations. In the present paper, these are applied to the elements discretizing the pile axis, pile shaft or suction caisson skirt.

2.4. Seismic input

The seismic action is a vertically incident (z-direction) S-wave that propagates through the stratified soil. Only an excitation in the x-direction is considered, so that the only non-null displacement at each layer j is:

$$u_x^{\mathrm{free},(j)}(z) = A^{(j)} e^{\mathrm{i}k^{(j)}z} + B^{(j)} e^{-\mathrm{i}k^{(j)}z} \tag{20}$$

where $A^{(j)}$ and $B^{(j)}$ are the amplitudes of the incident and reflected waves, $k^{(j)} = \omega / c_s^{(j)}$ is the wave number, and $c_s^{(j)} = \sqrt{\mu_{\mathrm{soil},j} / \rho_{\mathrm{soil},j}}$ is the shear wave propagation speed. The amplitudes are obtained from the one-dimensional wave propagation boundary value problem of a multilayered half-space.

The seismic action is inserted into the boundary element equations by decomposing the total field into the free-field and the scattered field:

$$u_k^{\mathrm{total}} = u_k^{\mathrm{free}} + u_k^{\mathrm{scattered}}, \ k = 1, 2, 3 \tag{21}$$

and then the scattered field $u_k^{\mathrm{total}} - u_k^{\mathrm{free}}$ is the one multiplying the integral kernels (see e.g. [37]).

In the case of pure finite element models (such as a rigid base model), the seismic action is directly introduced by imposing the prescribed displacements at the jacket bottom nodes.

3. Case studies

To illustrate the capabilities of the proposed integrated model, this section presents its application to a practical OWT case study under vertically incident S-waves. A comprehensive analysis is conducted considering different jacket configurations, foundations, and soil conditions. For comparison purposes, simpler models are also used: rigid base (no SSI) and flexible base using lumped springs/dashpots macroelements available in the classic literature (simple SSI).

3.1. Description of the analyzed cases

The wind turbine taken for the study is the DTU 10 MW Reference Wind Turbine, which is fully described in the corresponding report [39]. The rotor diameter D_{rotor} is 178.3 m. The RNA mass matrix and the tower model are obtained from the procedures described above and the data presented in the report. From the inertial point of view, only the total mass of the RNA ($m_{\mathrm{RNA}} = 770,180$ kg) is considered for building the RNA mass matrix. The tower a length of $h_{\mathrm{tower}} = 115.63$ m and a varying diameter and thickness, being $D_{\mathrm{tower-bottom}} = 8.3$ m and $t_{\mathrm{tower-bottom}} = 38$ mm at the bottom, and $D_{\mathrm{tower-top}} = 5.5$ m and $t_{\mathrm{tower-top}} = 20$ mm at the top.

The jackets used in the study are obtained from the preliminary design procedure described in [22], providing representative geometries to evaluate the modeling approach rather than final, practically feasible designs. As previously mentioned, three- and four-legged jackets are

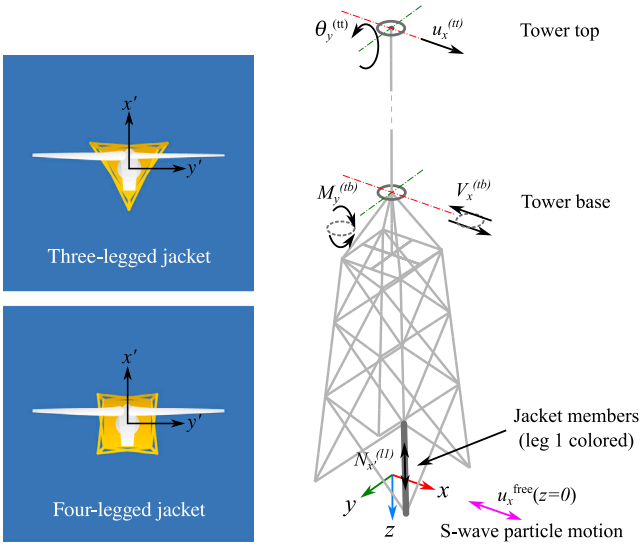

(a) Wind turbine orientation (b) Points of study along each jacket

Fig. 5. Definition of conventions and symbols used across the analyzed cases.

considered. Also, two sites with different water depths (20 and 50 m) but with the environmental conditions used in [22]. The resulting four jackets are fully described in Appendix A.

The relative orientation between the wind turbine and the jacket is shown in Fig. 5(a). The rotor rotation axis x' is parallel to the global x axis, and the z axis is located at the mudline level and pointing towards inside the soil, as shown in Fig. 2.

The soils to be studied correspond to the frontier between C ($180\,\mathrm{m/s} < c_{s,30} < 360,\mathrm{m/s}$) and D ($c_{s,30} < 180,\mathrm{m/s}$) soils [40], which are usually the type of soils where OWTs are founded on. In particular, a homogeneous soil with $c_s = 180\,\mathrm{m/s}$ (denoted as "hom180"), and a non-homogeneous soil with the following profile ($z \geq 0$):

$$c_s(z) = 90.5362 \cdot z^{0.312}\ \left[\mathrm{m/s}\right] \tag{22}$$

which also has $c_{s,30} = 180,\mathrm{m/s}$ (denoted as "nohom180") are considered. Constant density $\rho_{\mathrm{soil}} = 1800\,\mathrm{kg/m^3}$, Poisson's ratio $\nu_{\mathrm{soil}} = 0.35$ and hysteretic damping ratio $\xi_{\mathrm{soil}} = 5\%$ are assumed for all soils. This type of profiles is representative of offshore soils considered in several studies [41–43].

Each jacket is considered to be founded on piles or suction caissons. The main characteristics of the foundations have been taken from Sandal et al. [44], where similar jackets were studied. Piles have length $L = 35.1$ m, diameter $D = 2.59$ m, and shaft thickness $t = 3.22$ cm. Suction caissons have a length $L = 7.57$ m, diameter $D = 7.57$ m, and skirt thickness $t = 8.2$ cm.

The mechanical properties of the steel, assumed for all OWT components, are: density $\rho = 7850\ \mathrm{kg/m^3}$, Young's modulus $E = 210$ GPa, Poisson's ratio $\nu = 0.3$, and hysteretic damping ratio $\xi = 0.5\%$ ($E^* = E \cdot (1 + \mathrm{i}2\xi)$).

In addition to the proposed model, which is taken as the reference since it considers the soil stratigraphy and the complete three-dimensional SSI (soil–foundation and foundation–soil–foundation interaction), a fixed base model, i.e. no SSI interaction, and a lumped frequency-independent SSI model are used. The latter model uses lumped springs/dashpots with frequency-independent stiffnesses and viscous damping for each individual foundation mode: vertical, horizontal, rocking and torsional. This is a classical modeling approach, denoted here as "simple SSI". Only part of the SSI is included as no foundation–soil–foundation interaction is considered, and the seismic input filtering produced by the foundation system is neglected. According to the reference system shown in Fig. 4, the following impedance matrix representing the soil–foundation interaction is introduced at each jacket leg base node n_f:

$$\mathbf{K}^{(n_f)}\mathbf{a}^{(n_f)} = \left[\begin{pmatrix} k_h & 0 & 0 & 0 & -k_{SR} & 0 \\ 0 & k_h & 0 & k_{SR} & 0 & 0 \\ 0 & 0 & k_V & 0 & 0 & 0 \\ 0 & k_{SR} & 0 & k_R & 0 & 0 \\ -k_{SR} & 0 & 0 & 0 & k_R & 0 \\ 0 & 0 & 0 & 0 & 0 & k_T \end{pmatrix} + i\omega \begin{pmatrix} c_h & 0 & 0 & 0 & -c_{SR} & 0 \\ 0 & c_h & 0 & c_{SR} & 0 & 0 \\ 0 & 0 & c_V & 0 & 0 & 0 \\ 0 & c_{SR} & 0 & c_R & 0 & 0 \\ -c_{SR} & 0 & 0 & 0 & c_R & 0 \\ 0 & 0 & 0 & 0 & 0 & c_T \end{pmatrix}\right] \begin{pmatrix} u_x^{(n_f)} \\ u_y^{(n_f)} \\ u_z^{(n_f)} \\ \theta_x^{(n_f)} \\ \theta_y^{(n_f)} \\ \theta_z^{(n_f)} \end{pmatrix} \tag{23}$$

where k are the stiffnesses and c are the viscous damping coefficients related to the vertical (V), horizontal (H), rocking (R), sway-rocking (SR), and torsional (T) components. The values of these are adopted from the available literature as follows. For piles, they are taken from Novak & El Sharnouby [45]. For suction caissons, stiffnesses are taken from Doherty et al. [46] and viscous damping coefficients are taken from Gazetas [47]. The resulting stiffnesses and viscous damping coefficients are shown in Table 1.

The proposed model is formulated in the frequency domain and incorporates frequency-dependent matrices from the Boundary Element Method (BEM). Consequently, it is not possible to perform a standard eigenvalue modal analysis, as the system's properties vary with the excitation frequency. However, by looking at results in the frequency-domain it is possible to estimate how the resonant frequencies (especially the lower ones) and damping change between cases and modeling approaches. The frequency response is analyzed up to 10 Hz, which is the typical range of interest for seismic excitation. The seismic action is a vertically incident S-wave impinging in the x-direction (i.e., fore-aft direction, see Fig. 5(b)), and the following responses are studied:

- Tower top displacement and rotation.

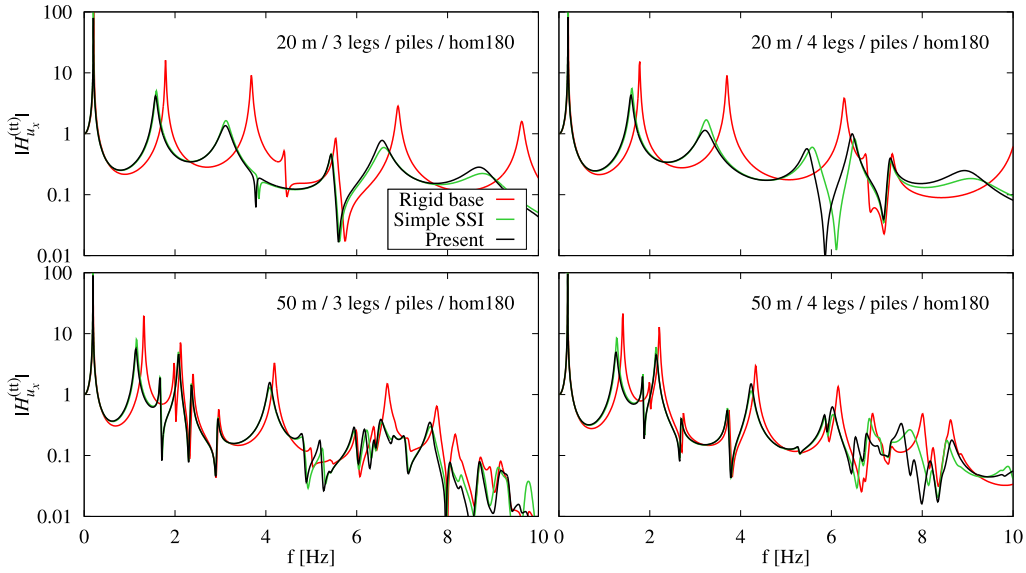

Fig. 6. Tower top normalized x displacement of OWT founded on piles on homogeneous soil.

Table 1
Summary of stiffnesses and viscous damping coefficients in the simple SSI for each type of foundation and type of soil.

Foundation	Piles		Suction caissons	
soil	hom180	nohom180	hom180	nohom180
k_V [GN/m]	2.711	2.090	2.484	2.775
c_V [MN s/m]	36.62	19.94	82.61	62.94
k_H [GN/m]	1.271	0.575	2.588	2.152
c_H [MN s/m]	21.78	10.16	49.46	37.68
k_R [GN m]	17.77	15.67	126.6	111.0
c_R [MN m s]	82.69	61.61	0	0
k_{SR} [GN]	3.302	2.369	10.29	10.83
c_{SR} [MN s]	33.42	20.92	0	0
k_T [GN m]	0	0	90.27	57.39
c_T [MN m s]	0	0	0	0

- Tower base shear and bending moment.
- Jacket legs and bracings axial forces.

This is illustrated in Fig. 5(b). At each case, the overall response over the considered frequency spectrum and the specific response at the fundamental frequency are separately discussed.

3.2. Tower top kinematic response

In the first place, the kinematic response (fore-aft displacement and rotation) at the tower top is studied. Figs. 6, 7, 8, 9 show the normalized absolute value of the x displacement for all the analyzed cases. Fig. 10 shows the normalized absolute value of the y rotation only for the case of pile foundations on homogeneous soil. Tower top rotation results for all other analyzed cases are included as supplementary material. Throughout the figures, normalized displacements and rotations are given by the following transfer functions:

$$H^{(tt)}_{u_x} = \frac{u^{(tt)}_x}{|u^{free}_x(z=0)|}\ [\mathrm{m/m}], \quad H^{(tt)}_{\theta_y} = \frac{\theta^{(tt)}_y}{|u^{free}_x(z=0)|}\ [1/\mathrm{m}] \tag{24}$$

The first row of graphs corresponds to 20 m water depth cases, and the second row corresponds to 50 m water depth cases. The first column of graphs corresponds to three-legged jackets and the second corresponds to four-legged jackets. Due to the symmetry of the configuration and the excitation, the y displacement (side-side) and the z rotation (OWT torsional response) are both null at the tower top.

3.2.1. Response along the analyzed frequency range

Overall, results presented in Figs. 6 to 10 show that the fundamental frequency in each case is well-captured even by the rigid base model. A more detailed analysis at the fundamental frequency is given later. As expected, SSI becomes more relevant as the frequency increases, and it produces an important reduction of higher natural frequencies and an increase of damping, which are two well-known SSI effects.

When comparing the first and second rows of plots in Figs. 6 to 10 (corresponding to OWT for 20 m and 50 m water depths), it is observed that SSI is less relevant as the substructure height increases. This behavior is reasonable because common individual foundation dimensions have been assumed, while the spacing between the foundations is larger in the 50 m depth case and it is known that the foundation system rocking impedance increases with the squared spacing [48]. Also, the results in the second row of Figs. 6 to 10 show that the response in all 50 m water depth cases is much more complex, exhibiting additional resonance peaks and higher modal contributions. This behavior is due to the presence of jacket local vibration modes related to bracings and legs. Such a result is reasonable since members of 50 m water depth jackets are longer than members of 20 m water depth jackets.

From the SSI modeling point of view, it may seem that differences between SSI modeling approaches shown in Figs. 6 to 10 are small, but this is only in appearance as ordinates in these graphs are presented in logarithmic scale. In these figures, it can be observed that simple SSI models (frequency independent springs/dashpots) work reasonably well for frequencies below 2 Hz, where the curves for both models nearly overlap, but beyond this frequency there are important differences. Simple SSI models for pile and suction caissons in homogeneous soils work remarkably well within the analyzed frequency window, as shown respectively in Figs. 6 and 7, although there are several noticeable discrepancies at high frequencies. The discrepancies between the present model and the simple SSI becomes quite large for the non-homogeneous cases (Figs. 8 and 9). This may be due to the particular stiffnesses and viscous damping coefficients taken from the available literature, and/or due to the limitations behind a spring/dashpot model with constant parameters. Therefore, it reveals the importance of choosing the appropriate constants from the literature (if available for the case under study) and the uncertainty behind this selection. It also reveals the relevance of using a direct coupled model such as the presented one.

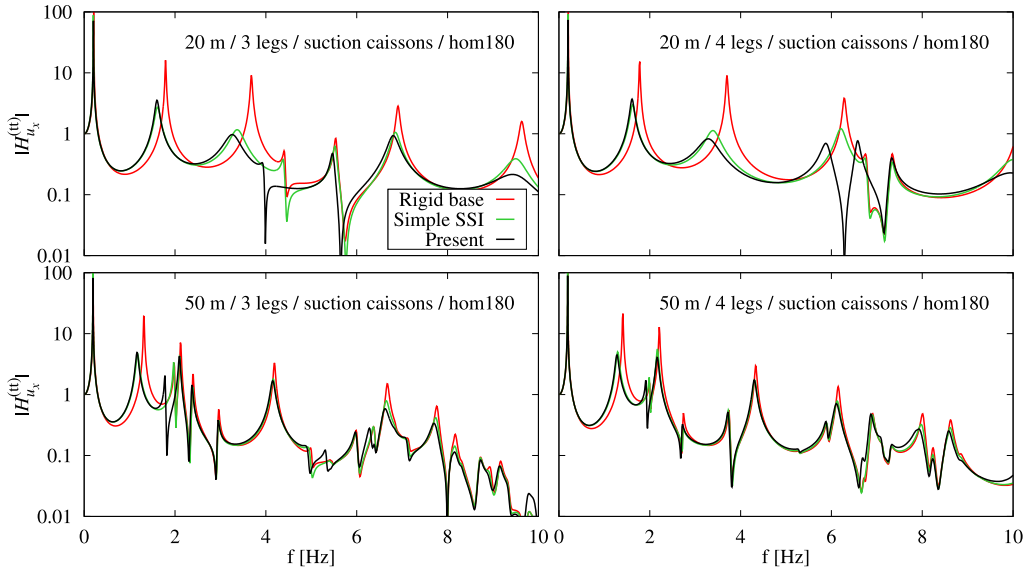

Fig. 7. Tower top normalized x displacement of OWT founded on suction caissons on homogeneous soil.

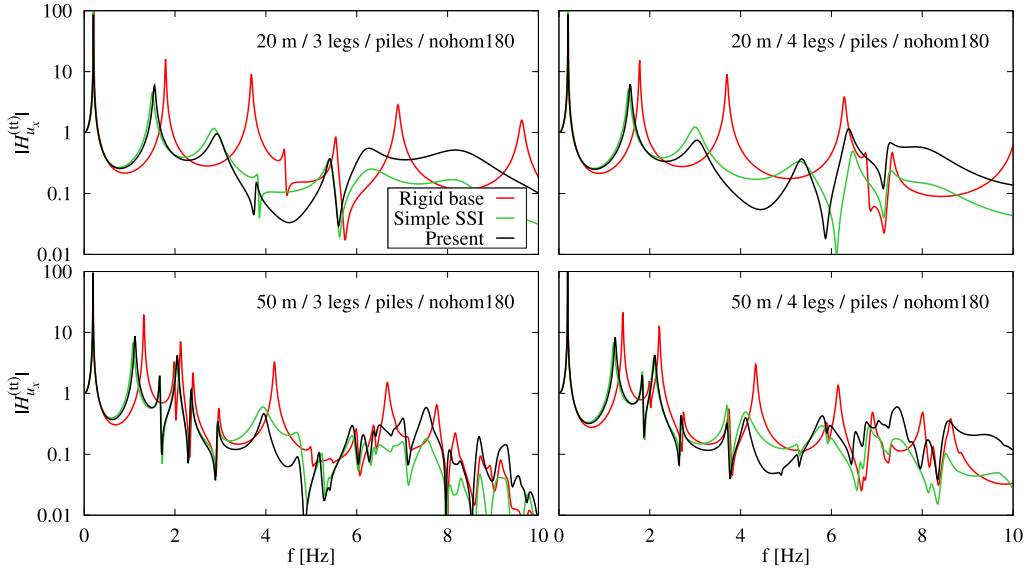

Fig. 8. Tower top normalized x displacement of OWT founded on piles on non-homogeneous soil.

All the above discussion applies to both the fore-aft displacement and rotation results. The only remarkable difference is the fact that the magnitude of the rotational response decreases much less than the translational response with SSI, as can be observed when comparing Fig. 6 against Fig. 10. The relevance of RNA rotation lies on the fact that it is a limited by current serviceability limit states in order to avoid blade-tower impact, typically by 0.5 degrees [49].

3.2.2. *Response at the fundamental frequency*

Finally, let us now dive into the analysis at the fundamental frequency in each case. The fundamental frequency is of paramount importance because it has to be located inside a frequency window between the rotor (1P) and blade-passing (3P) frequencies in order to reduce fatigue as much as possible [49]. It is also important to analyze what happens to the magnitude of the response, which is directly related to the damping. In order to give an idea, Fig. 11 shows the real and imaginary parts of the translational and rotational responses around the fundamental frequency of a specific case (20 m water depth, 4 piles and homogeneous soil). In previous plots this went unnoticed, but a 3.3% reduction of the fundamental frequency f_1 from 0.2057 Hz (rigid base) to 0.1989 Hz (simple SSI model) and 0.1987 Hz (SSI with the present model) is observed. At the same time, SSI models estimate peak displacements and rotations that are 25% smaller than those predicted by the fixed-base model. This means that even the simple SSI model predicts quite well the fundamental frequency, but greatly underestimates damping. This is presumably due to the use of viscous damping in the simple SSI model, while the present model uses hysteretic damping. These trends are observed in all cases, as it is described next.

Table 2 and Fig. 12 present the fundamental frequency of all analyzed cases, taken from the fore-aft displacement response, as well as the fundamental frequency difference with respect to rigid base cases. The fundamental frequency in these cases ranges between 0.19 and 0.21 Hz, which is lower than the fundamental frequency of 0.25 Hz [39] of the tower and RNA alone (approximately 20% reduction). This reduction indicates the crucial role of the jacket design and

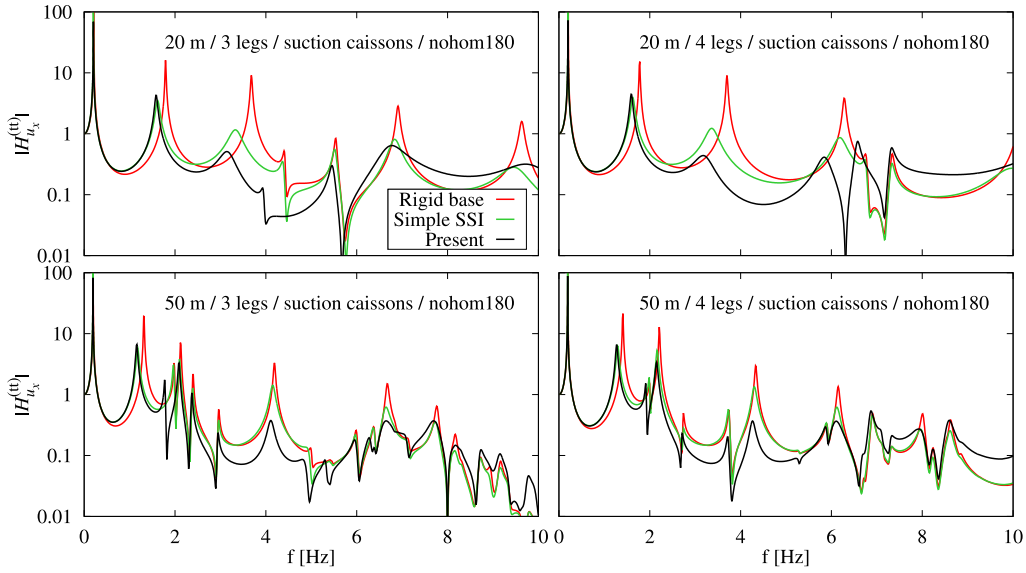

Fig. 9. Tower top normalized x displacement of OWT founded on suction caissons on non-homogeneous soil.

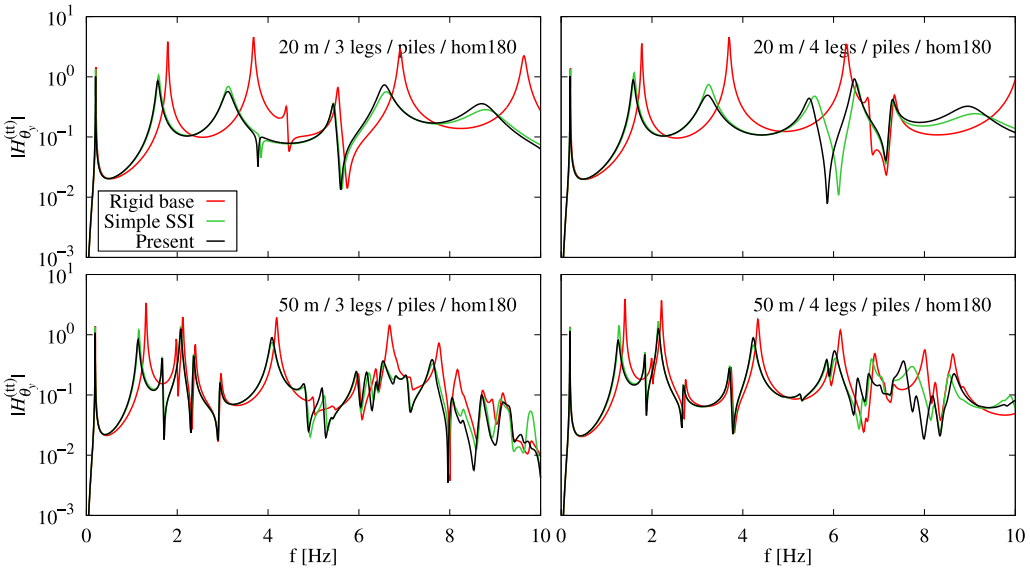

Fig. 10. Tower top normalized y rotation of OWT founded on piles on homogeneous soil.

analysis for achieving an appropriate fundamental frequency located inside the available frequency window between 1P and 3P frequencies. The impact of SSI modeling for predicting the fundamental frequency seems small (4.9% in the worst case), but softer soils than those considered here may also be encountered in practice. Furthermore and most importantly, DNV suggests that f_1 should be at least 10% away from the 1P and 3P frequencies [50], which means that these modeling discrepancies can be quite relevant.

The results obtained are comparable to those obtained in other references. For the same wind turbine (tower and RNA), but different jacket, foundation and soil, the fundamental frequency reported in [51, Table 4] is 0.23 Hz (without SSI) and 0.21 Hz (with SSI).

Table 3 and Fig. 13 present the magnitude of the peak displacements at the tower top at the fundamental frequency for all analyzed cases, as well as their difference with respect to rigid base cases. The material and geometrical damping introduced by the foundation–soil system plays a significant role in reducing the peak magnitude. From Table 3, it is observed that suction caisson foundations introduce more damping than pile foundations. Also, results show that 50 m water depth cases present less damping that the respective 20 m water depth cases. Regarding SSI modeling, both the fixed base and the simple SSI approach greatly underestimates damping in all cases, leading to very conservative results.

3.3. Tower base shear force and bending moment response

In this section, the fore-aft tower base shear force and bending moment are studied. Figs. 14 and 15 show respectively the normalized fore-aft shear force (V_x) and bending moment (M_y), only for the cases of suction caisson foundations on non-homogeneous soils. Results for all other analyzed cases are included as supplementary material. Throughout these figures, normalized shear forces and bending moments are given by the following transfer functions:

$$H_{V_x}^{(\mathrm{tb})} = \frac{V_x^{(\mathrm{tb})}}{|u_x^{\mathrm{free}}(z=0)|}\ [\mathrm{N/m}], \quad H_{M_y}^{(\mathrm{tb})} = \frac{M_y^{(\mathrm{tb})}}{|u_x^{\mathrm{free}}(z=0)|}\ [\mathrm{N\ m/m}] \tag{25}$$

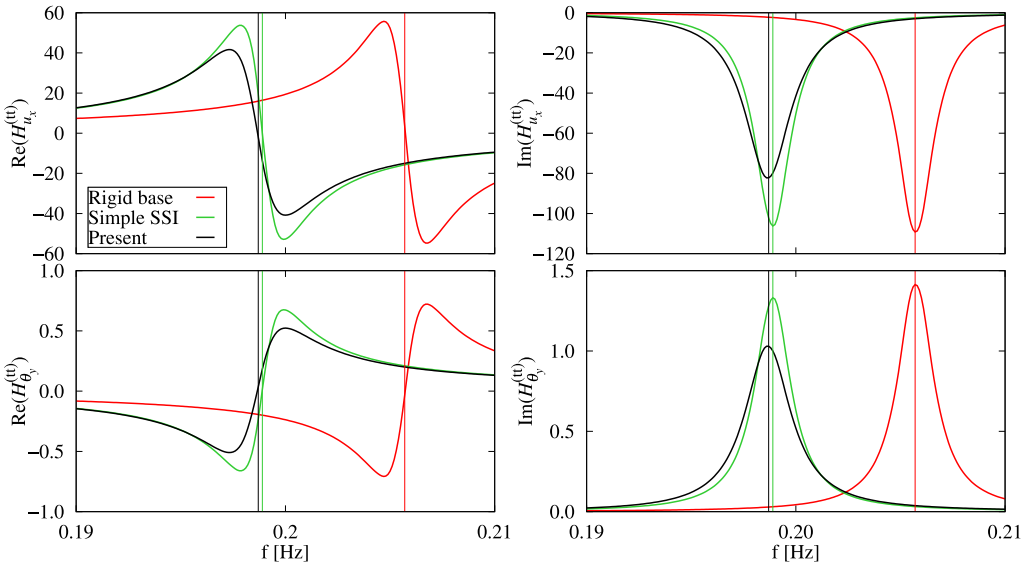

Fig. 11. Tower top normalized x displacement and y rotation around the fundamental frequency of 20 m water depth OWT founded on 4 piles on homogeneous soil with $c_s = 180$ m/s under S-waves impinging in the x-direction.

Table 2
Fundamental frequency f_1 (in Hz) of all analyzed cases and types of SSI modeling.

Soil	Found.	SSI mod.	$f_1/\left[(f_1 - f_1^{\text{rigid base}})/f_1^{\text{rigid base}}\right]$			
			20 m 3 legs	20 m 4 legs	50 m 3 legs	50 m 4 legs
–	–	Rigid base	0.2110	0.2057	0.1981	0.1947
hom180	piles	Simple SSI	0.2031/−3.7%	0.1989/−3.3%	0.1936/−2.3%	0.1918/−1.5%
		Present	0.2029/−3.8%	0.1987/−3.4%	0.1931/−2.5%	0.1915/−1.6%
	caissons	Simple SSI	0.2027/−3.9%	0.1986/−3.5%	0.1933/−2.4%	0.1917/−1.5%
		Present	0.2040/−3.3%	0.1997/−2.9%	0.1937/−2.2%	0.1919/−1.4%
nohom180	piles	Simple SSI	0.2006/−4.9%	0.1967/−4.4%	0.1920/−3.1%	0.1907/−2.1%
		Present	0.2030/−3.8%	0.1987/−3.4%	0.1933/−2.4%	0.1916/−1.6%
	caissons	Simple SSI	0.2034/−3.6%	0.1992/−3.2%	0.1937/−2.2%	0.1919/−1.4%
		Present	0.2033/−3.6%	0.1991/−3.2%	0.1935/−2.3%	0.1918/−1.5%

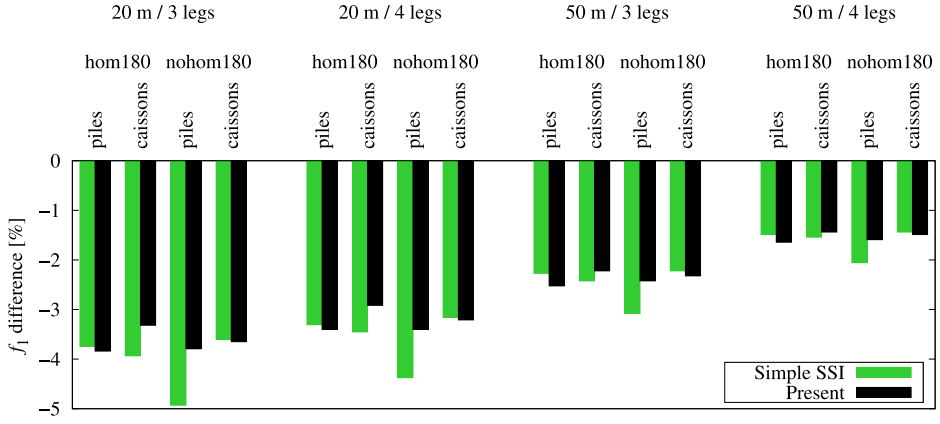

Fig. 12. Fundamental frequency f_1 differences with respect to rigid base cases.

Regarding the relevance of SSI modeling, tower base shear force and bending moment follow trends similar to those observed for the tower top kinematic response. For frequencies beyond the fundamental frequency, the differences due to SSI modeling are quite large. For example, in the cases of 20 m water depth jackets, the magnitude of the peaks corresponding to second and third modes of vibration decreases very significantly when SSI is taken into account due to the effect of material and radiation damping in the soil–foundation system. Depending on the specific case, differences between results from simple SSI model and the present model are very large (one order of magnitude)

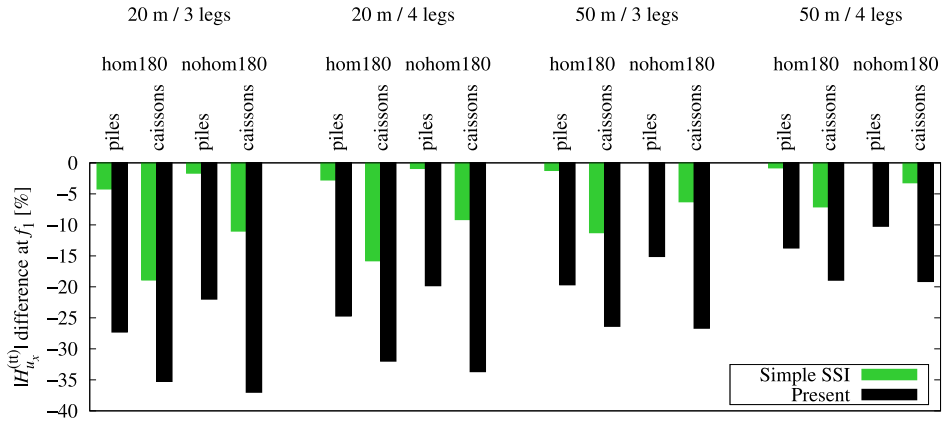

Fig. 13. Differences of the tower top displacement peak magnitude at f_1 with respect to rigid base cases.

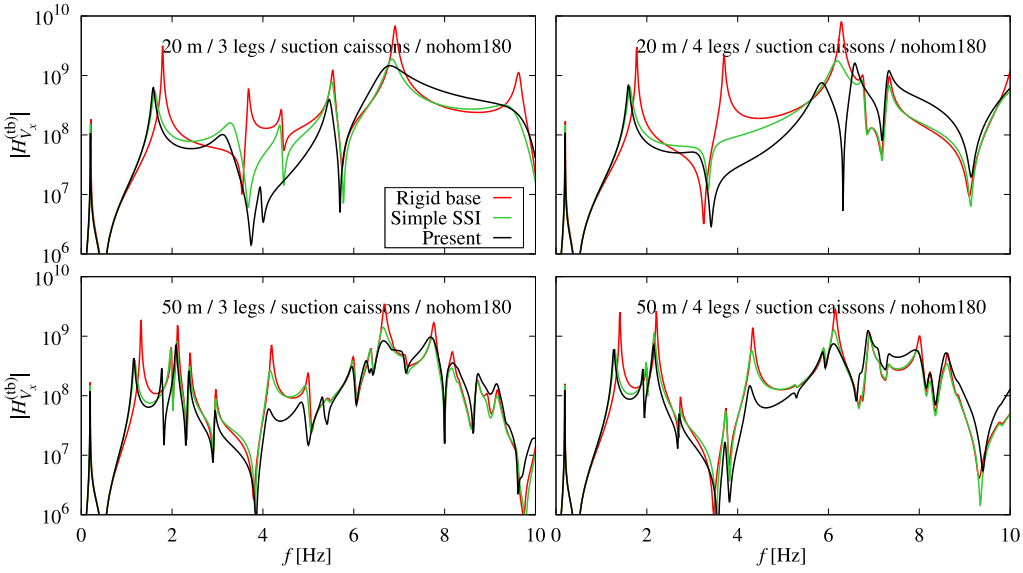

Fig. 14. Tower base normalized shear force of OWT founded on suction caissons on non-homogeneous soil.

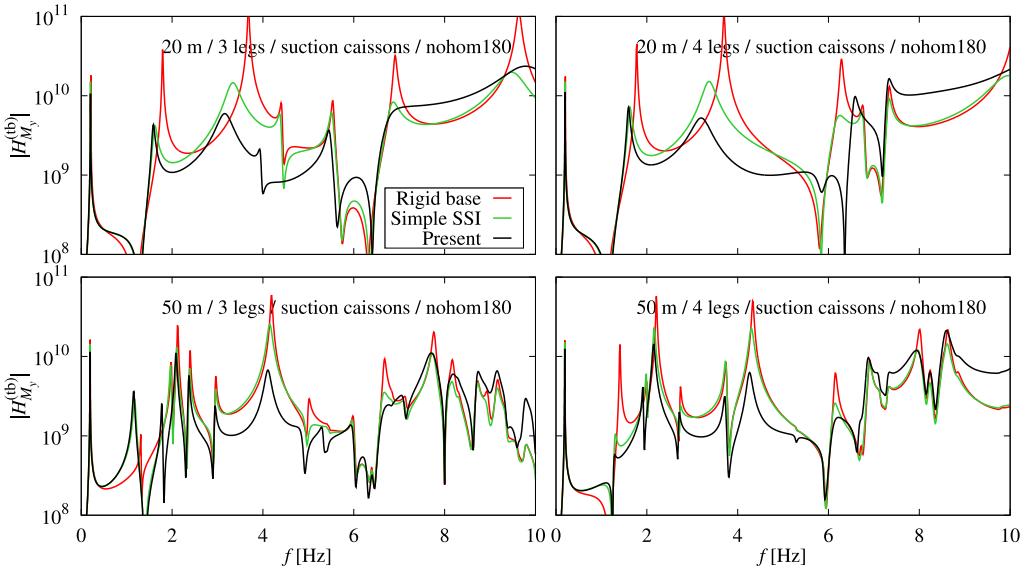

Fig. 15. Tower base normalized bending moment of OWT founded on suction caissons on non-homogeneous soil.

Table 3
Tower top displacement peak magnitude at f_1 of all analyzed cases and types of SSI modeling.

Soil	Found.	SSI mod.	$\lvert H^{(tt)}_{u_x}\rvert / \left[\left(\lvert H^{(tt)}_{u_x}\rvert - \lvert H^{(tt)}_{u_x}\rvert^{\text{rigid base}}\right) / \lvert H^{(tt)}_{u_x}\rvert^{\text{rigid base}}\right]$ at f_1			
			20 m 3 legs	20 m 4 legs	50 m 3 legs	50 m 4 legs
–	–	Rigid base	110.1	109.2	112.3	110.8
hom180	piles	Simple SSI	105.5/−4.2%	106.2/−2.7%	111.0/−1.2%	109.9/−0.8%
		Present	80.1/−27.2%	82.2/−24.7%	90.3/−19.6%	95.6/−13.7%
	caissons	Simple SSI	89.3/−18.9%	92.0/−15.8%	99.7/−11.2%	103.0/−7.0%
		Present	71.3/−35.2%	74.3/−32.0%	82.7/−26.4%	89.9/−18.9%
nohom180	piles	Simple SSI	108.3/−1.6%	108.2/−0.9%	113.4/1.0%	111.1/0.2%
		Present	86.0/−21.9%	87.6/−19.8%	95.4/−15.0%	99.5/−10.2%
	caissons	Simple SSI	98.0/−11.0%	99.2/−9.2%	105.3/−6.2%	107.3/−3.2%
		Present	69.4/−37.0%	72.4/−33.7%	82.4/−26.6%	89.6/−19.1%

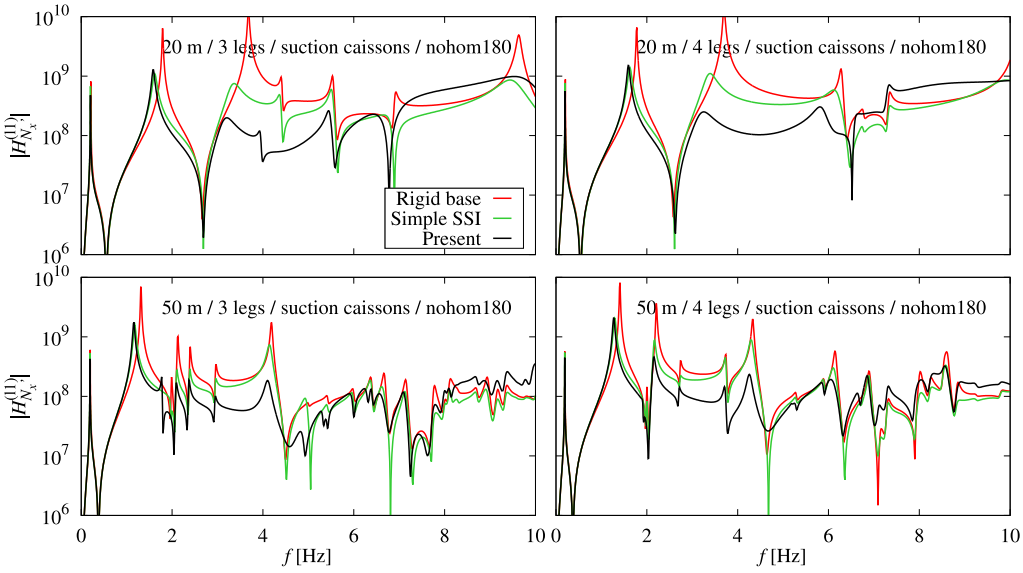

Fig. 16. Jacket leg 1 ($x > 0$, $y > 0$) normalized axial force ($H^{(11)}_{N_{x'}}$) of OWT founded on suction caissons on non-homogeneous soil.

within the 2–5 Hz frequency window. However, the relevance of these differences on the time-domain response will depend on the frequency content of the specific earthquake. The response in terms of frequencies was already discussed in detail in previous sections. The trends already observed before can again be seen here.

3.4. Jacket legs and bracings axial force response

In this section, the impact of SSI on the dynamic response of the jacket is studied by analyzing axial forces in legs and bracings. Fig. 16 shows the absolute value of the normalized axial force ($N_{x'}$) at the lowest part of jacket leg 1 (leg located on $x > 0$, $y > 0$) for the cases of suction caisson foundations on non-homogeneous soil. Results for all other analyzed cases are included as supplementary material. Throughout these figures, the normalized axial force is given by the following transfer function:

$$H^{(11)}_{N_{x'}} = \frac{N^{(11)}_{x'}}{|u^{\text{free}}_x(z=0)|} \text{ [N/m]} \tag{26}$$

The global flexural behavior of a jacket structure is governed by axial forces along the legs, which resist the global bending moment, while axial forces in bracings resist the global shear force. Despite the dynamic nature of this analysis and the geometric complexity of the jackets (e.g., a typical leg batter of 1:8 and varying member cross-sections), this fundamental working principle remains valid. Consequently, the results exhibit trends similar to those observed in previous cases. However, the 50 m jackets show a significantly more complex response, presumably due to the interaction of local vibration modes within the jacket members.

Following the path established in previous sections, the response at the fundamental frequency was analyzed in detail regarding the axial force distribution throughout the jacket. Since the number of jacket members is large, figures showing colored members according to their peak value (imaginary part of the normalized axial force) for each SSI model, and also figures illustrating the relative difference between the present approach and simple SSI approach with respect to the rigid base case have been produced. Here, Figs. 17 and 18 depict the relative differences for the particular case of a 50 m water depth jacket founded respectively on 3 and 4 suction caissons on non-homogeneous soil. The remaining results are provided in the supplementary material. Analysis of all cases reveals several notable observations.

First, all cases exhibit a peak reduction in jacket legs when SSI is included, and the reduction values coincide with those of the tower top displacement and the tower base bending moment. This is reasonable given the jacket working mechanism discussed in the previous paragraph.

Second, there is a strong influence of SSI modeling on the axial forces of bracings, especially for those near the foundation. In particular, for all jacket heights and number of legs, the lowest bracing normal to the excitation direction exhibit a much smaller axial force when SSI is included. This may be explained by observing that both legs facing the excitation direction are either in compression or in tension, and

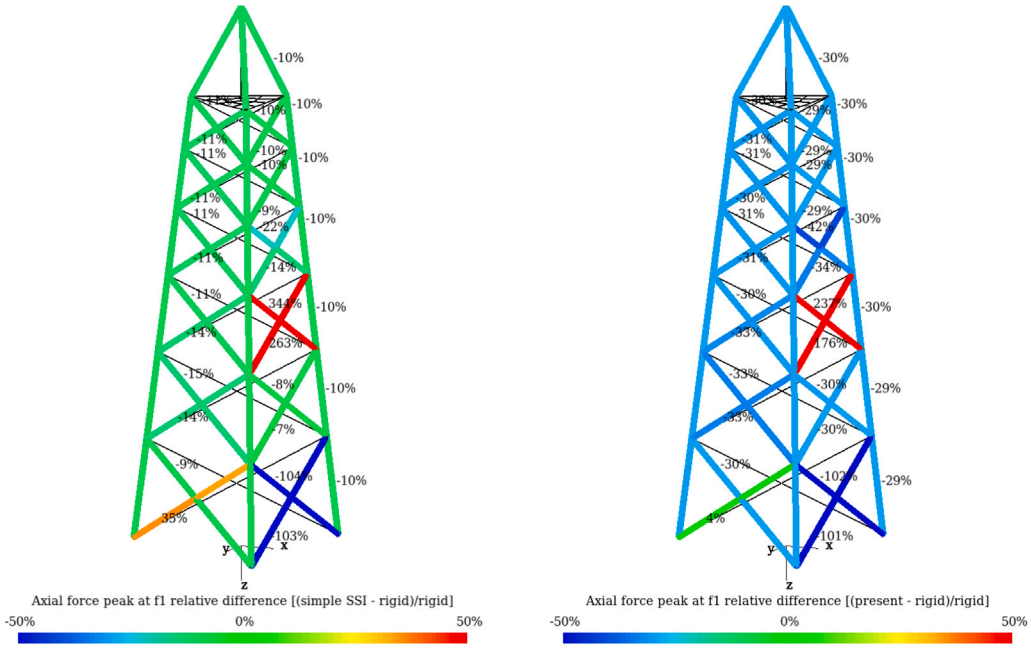

(a) Simple SSI approach against rigid base (b) Present approach against rigid base

Fig. 17. Relative differences of axial force peak values at f_1 between SSI modeling approaches. Jacket of 50 m height founded on 3 suction caissons on non-homogeneous soil.

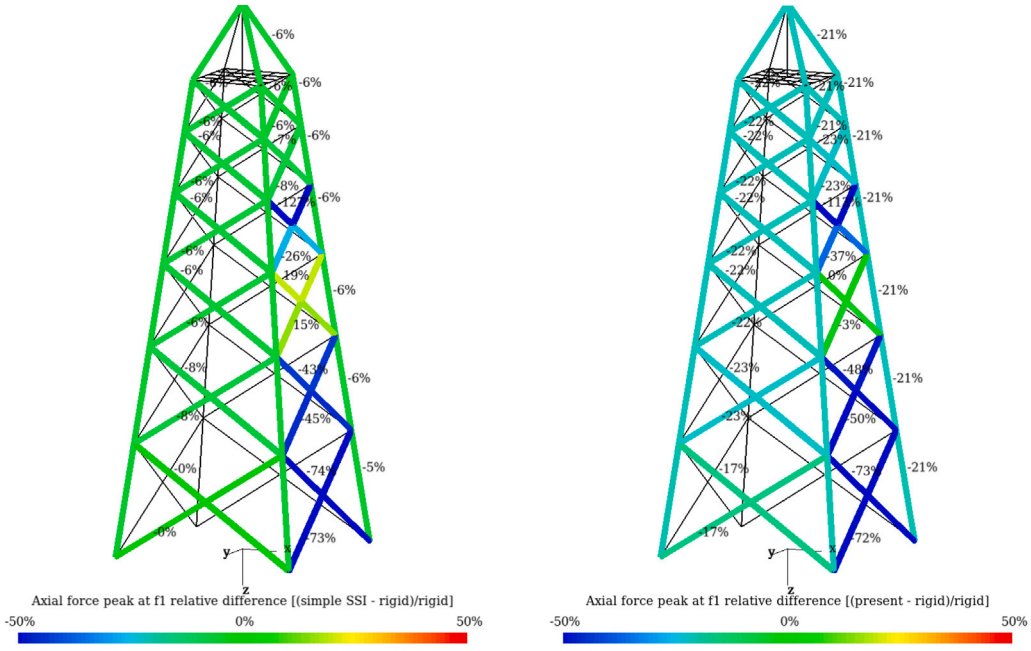

(a) Simple SSI approach against rigid base (b) Present approach against rigid base

Fig. 18. Relative differences of axial force peak values at f_1 between SSI modeling approaches. Jacket of 50 m height founded on 4 suction caissons on non-homogeneous soil.

restraining the leg displacement (rigid base case) produces higher axial forces due to the Poisson effect. On the other hand, the lowest bracing at 30 degrees (for 3 legs cases) or parallel (for 4 legs cases) to the excitation direction usually experiences higher axial forces when SSI is included, effect which is present in all 3-legged jacket cases.

Overall, the structural response of bracings when considering SSI approximates the baseline values of the legs at upper bracing levels. Finally, it should be pointed out that these conclusions are limited to the topology considered here, i.e. X-bracing without horizontal members.

4. Conclusions and further research

This paper has presented an integrated direct soil–structure model for the seismic analysis of Offshore Wind Turbines (OWTs) supported by jacket substructures. By combining Timoshenko beam and Reissner–Mindlin shell finite elements with a rigorous boundary element formulation for stratified soil, the proposed model captures the complex Soil–Structure Interaction (SSI) phenomena essential for accurate dynamic assessment of these structures. The main contributions and findings of this work can be summarized as follows:

- A coupled model of the wind turbine, transition piece, jacket, and foundation (piles or suction caissons) in non-homogeneous soils within a frequency-domain framework is proposed. This direct formulation avoids any of the traditional simplifications, allowing for a more natural and rigorous treatment of the problem.
- A comprehensive comparative study of different SSI modeling approaches (rigid base, simple engineering SSI, and the present model) has been performed for obtaining the response of OWTs with different jacket heights (20 m, 50 m), number of legs (3, 4), type of foundations (piles, suction caissons), and homogeneous and non-homogeneous soils.
- Several typical SSI effects such as natural frequency reduction and damping increase are observed. These effects have been quantified using the present and the simple SSI engineering approaches.
- The use of springs/dashpots (simple SSI) taken from the literature for the particular soil–foundation system under analysis is simple and effective. However, since these are typically obtained for idealized soil profiles for isolated foundations, results may be unreliable and they should be used only when SSI influence in the system is relatively small.

While the present approach is a robust framework for seismic linear analysis, two main lines for future research remain:

- Study of the practical impact of SSI modeling on the time-domain structural response of the jacket substructure by considering a comprehensive earthquake database and different types of soils.
- Further development of the model by incorporating a Green's functions for horizontally layered poroelastic half-space under an inviscid fluid layer.

CRediT authorship contribution statement

J.D.R. Bordón: Writing – review & editing, Writing – original draft, Software, Methodology, Investigation, Formal analysis, Data curation, Conceptualization. **R. Quevedo-Reina:** Writing – review & editing, Software, Resources, Investigation, Data curation. **G.M. Álamo:** Writing – review & editing, Methodology, Conceptualization. **C. Medina:** Writing – review & editing, Methodology. **L.A. Padrón:** Writing – review & editing, Supervision, Funding acquisition. **J.J. Aznárez:** Writing – review & editing, Writing – original draft, Supervision, Methodology, Investigation, Funding acquisition, Conceptualization. **O. Maeso:** Writing – review & editing, Supervision, Resources, Funding acquisition.

Declaration of competing interest

The authors declare that they have no known competing financial interests or personal relationships that could have appeared to influence the work reported in this paper.

Acknowledgments

This study was supported by the Ministerio de Ciencia, Innovación y Universidades and the Agencia Estatal de Investigación (MICIU/AEI/10.13039/501100011033) of Spain and ERDF/EU through Research Project PID2023-151635OB-I00.

Appendix A. Description of jackets used in the study

The jackets analyzed in this study follow the preliminary design procedure described by Quevedo et al. [22]. These structures are X-braced with a constant bracing angle along their height and no horizontal members. Designed for water depths of 20 m and 50 m, the jackets assume environmental conditions similar to the previous work, and the obtained geometry is illustrated in Fig. A.19. All structural members

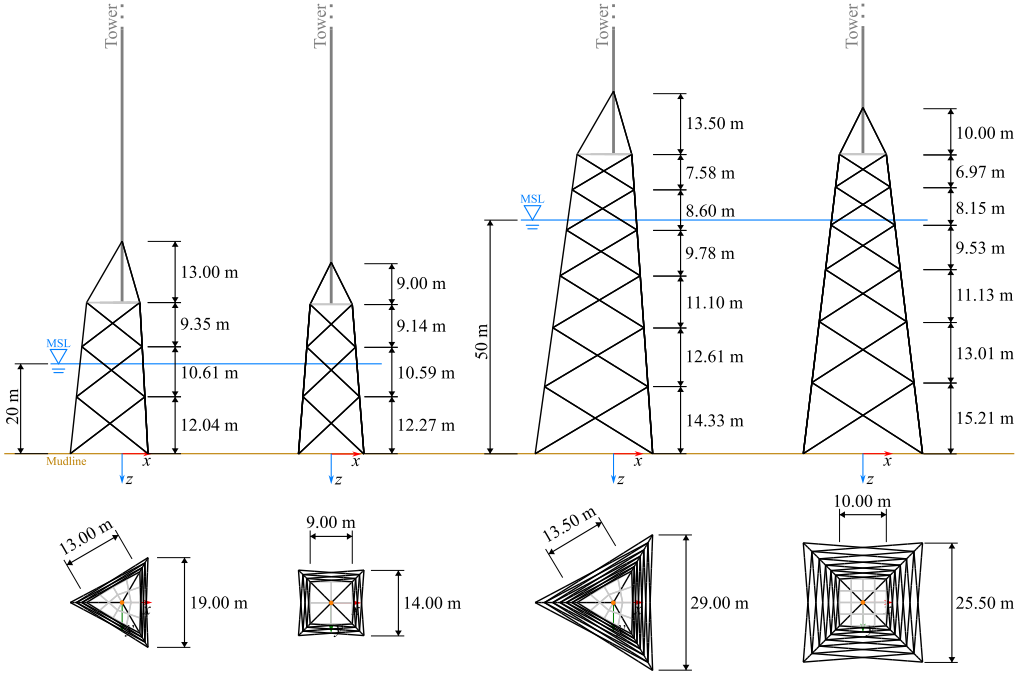

Fig. A.19. Geometry of three- and four-legged jackets for 20 m and 50 m water depths.

Table A.4
Cross section detail for each jacket design. All members have circular hollow sections with outer diameter D and thickness t, both given in mm.

Member type	20 m 3 legs		20 m 4 legs		50 m 3 legs		50 m 4 legs	
	D	t	D	t	D	t	D	t
Legs and top strut	1945	33	1871	31.5	1848	31	1652	27.5
Bracing 1 (lowest)	733	12	774	13	672	11	554	9.5
Bracing 2	774	13	607	10	619	10.5	562	9.5
Bracing 3	847	14.5	643	10.5	599	10	588	13
Bracing 4					993	16.5	829	14
Bracing 5					745	12.5	545	9
Bracing 6 (highest)					765	13	976	16.5

consist of Circular Hollow Sections (CHS). While the legs and top struts have the same cross-section within each design, the bracing cross-sections are constant at each level but vary across the total height of the jacket. Table A.4 contains the cross-sections used in each case.

Appendix B. Supplementary data

Supplementary material related to this article can be found online at https://doi.org/10.1016/j.enganabound.2026.106822.

Data availability

Data will be made available on request.

References

[1] Bhattacharya S, Nikitas G. 8 - wind energy: status and outlook with focus on offshore wind. In: Letcher TM, Fthenakis VM, editors. Energy and climate change. Academic Press; 2025, p. 197–224. http://dx.doi.org/10.1016/B978-0-443-21927-6.00014-3.

[2] Council GWE. Global Offshore Wind Report 2025. Tech. rep., Brussels, Belgium: GWEC; 2025.

[3] Kim Y-J, Lim JS, Kim HJ, Choi S-W. A comprehensive review of foundation designs for fixed offshore wind turbines. Int J Nav Archit Ocean Eng 2025;17:100643. http://dx.doi.org/10.1016/j.ijnaoe.2025.100643.

[4] Bhattacharya S. Design of foundations for offshore wind turbines. Hoboken, NJ, USA: John Wiley & Sons; 2019, http://dx.doi.org/10.1002/9781119128137.

[5] WindEurope. Wind energy in Europe 2024. Statistics and the outlook for 2025–2030. 2025.

[6] Domínguez J, Roesset JM. Dynamic stiffness of rectangular foundations. (R78-20). Cambridge, Massachusetts 02139: Massachusetts Institute of Technology, Department of Civil Engineering, Constructed Facilities Division; 1978, Sponsored by the National Science Foundation under Grant NSF RANN ENV 77-18339; NTIS Accession No. PB287131.

[7] Domínguez J, Roesset JM. Response of embedded foundations to travelling waves. (R78-24). Cambridge, Massachusetts 02139: Massachusetts Institute of Technology, Department of Civil Engineering, Constructed Facilities Division; 1978, Sponsored by the National Science Foundation under Grant NSF-RANN ENV 77-18339; NTIS Accession No. PB287130.

[8] Abascal R, Domínguez J. Vibrations of footings on zoned viscoelastic soils. J Eng Mech 1986;112(5):433–47. http://dx.doi.org/10.1061/(ASCE)0733-9399(1986)112:5(433).

[9] Alarcón E, Cano JJ, Domínguez J. Boundary element approach to the dynamic stiffness functions of circular foundations. Int J Numer Anal Methods Geomech 1989;13(6):645–64. http://dx.doi.org/10.1002/nag.1610130606.

[10] Emperador JM, Domínguez J. Dynamic response of axisymmetric embedded foundations. Earthq Eng Struct Dyn 1989;18(8):1105–17. http://dx.doi.org/10.1002/eqe.4290180803.

[11] Medina F, Domínguez J, Tassoulas JL. Response of dams to earthquakes including effects of sediments. J Struct Eng 1990;116(11):3108–21. http://dx.doi.org/10.1061/(ASCE)0733-9445(1990)116:11(3108).

[12] Japón BR, Gallego R, Domínguez J. Dynamic stiffness of foundations on saturated poroelastic soils. J Eng Mech 1997;123(11):1121–9. http://dx.doi.org/10.1061/(ASCE)0733-9399(1997)123:11(1121).

[13] Maeso O, Aznárez JJ, Domínguez J. Effects of space distribution of excitation on seismic response of arch dams. J Eng Mech 2002;128(7):759–68. http://dx.doi.org/10.1061/(ASCE)0733-9399(2002)128:7(759).

[14] Galvín P, Romero A, Domínguez J. Fully three-dimensional analysis of high-speed train–track–soil-structure dynamic interaction. J Sound Vib 2010;329(24):5147–63. http://dx.doi.org/10.1016/j.jsv.2010.06.016.

[15] Galvín P, Romero A, Solís M, Domínguez J. Dynamic characterisation of wind turbine towers account for a monopile foundation and different soil conditions. Struct Infrastruct Eng 2017;13(7):942–54. http://dx.doi.org/10.1080/15732479.2016.1227342.

[16] Álamo GM, Aznárez JJ, Padrón LA, Martínez-Castro AE, Gallego R, Maeso O. Dynamic soil-structure interaction in offshore wind turbines on monopiles in layered seabed based on real data. Ocean Eng 2018;156:14–24. http://dx.doi.org/10.1016/j.oceaneng.2018.02.059.

[17] Dong RG. Effective mass and damping of submerged structures. Tech. Rep. UCRL-52342, Lawrence Livermore Laboratory; 1978.

[18] Pak RYS, Guzina BB. Three-dimensional green's functions for a multilayered half-space in displacement potentials. J Eng Mech 2002;128(4):449–61. http://dx.doi.org/10.1061/(ASCE)0733-9399(2002)128:4(449).

[19] Padrón LA, Aznárez JJ, Maeso O. BEM–FEM coupling model for the dynamic analysis of piles and pile groups. Eng Anal Bound Elem 2007;31(6):473–84. http://dx.doi.org/10.1016/j.enganabound.2006.11.001.

[20] Álamo GM, Martínez-Castro AE, Padrón LA, Aznárez JJ, Gallego R, Maeso O. Efficient numerical model for the computation of impedance functions of inclined pile groups in layered soils. Eng Struct 2016;126:379–90. http://dx.doi.org/10.1016/j.engstruct.2016.07.047.

[21] Bordón JDR, Aznárez JJ, Maeso O. Dynamic model of open shell structures buried in poroelastic soils. Comput Mech 2017;60(2):269–88. http://dx.doi.org/10.1007/s00466-017-1406-3.

[22] Quevedo-Reina R, Álamo GM, François S, Lombaert G, Aznárez JJ. Importance of the soil–structure interaction in the optimisation of the jacket designs of offshore wind turbines. Ocean Eng 2024;303:117802. http://dx.doi.org/10.1016/j.oceaneng.2024.117802.

[23] Skjoldan P, Hansen M. On the similarity of the coleman and Lyapunov–floquet transformations for modal analysis of bladed rotor structures. J Sound Vib 2009. http://dx.doi.org/10.1016/j.jsv.2009.07.007.

[24] LPTV subspace analysis of wind turbine data. In: vol.7th European Workshop on Structural Health Monitoring. La Cité, Nantes, France: Inria; 2014.

[25] Acar GD, Feeny BF. Floquet-type analysis of transient vibrations of a horizontal axis wind turbine. In: Mains M, Dilworth B, editors. Topics in modal analysis & testing, volume 9. Conference proceedings of the society for experimental mechanics series, vol. 9, Cham, Switzerland: Springer; 2019, p. 329–33. http://dx.doi.org/10.1007/978-3-319-74700-2_37.

[26] Friedman Z, Kosmatka JB. An improved two-node Timoshenko beam finite element. Comput Struct 1993;47(3):473–81. http://dx.doi.org/10.1016/0045-7949(93)90243-7.

[27] Bucalem ML, Bathe KJ. Higher-order MITC general shell elements. Internat J Numer Methods Engrg 1993;36:3729–54. http://dx.doi.org/10.1002/nme.1620362109.

[28] Cowper GR. The shear coefficient in timoshenko's beam theory. J Appl Mech 1966;33(2):335–40. http://dx.doi.org/10.1115/1.3625046.

[29] Ali A, De Risi R, Sextos A. Seismic assessment of wind turbines: How crucial is rotor-nacelle-assembly numerical modeling? Soil Dyn Earthq Eng 2021;141:106483. http://dx.doi.org/10.1016/j.soildyn.2020.106483.

[30] Lee Y-S, González JA, Lee JH, Kim YI, Park KC, Han S. Structural topology optimization of the transition piece for an offshore wind turbine with jacket foundation. Renew Energy 2016;85:1214–25. http://dx.doi.org/10.1016/j.renene.2015.07.052.

[31] Rudzki P. Steel jackets on a barge (1). 2017, CC0 1.0 Universal Public Domain Dedication. Available at URL https://commons.wikimedia.org/wiki/File:Steel_jackets_on_a_barge_(1).jpg. [Accessed 15January 2026].

[32] Damiani R. JacketSE: An Offshore Wind Turbine Jacket Sizing Tool; Theory Manual and Sample Usage with Preliminary Validation. Tech. Rep. NREL/TP-5000-65417, Golden, CO: National Renewable Energy Laboratory (NREL); 2016, http://dx.doi.org/10.2172/1238573.

[33] Álamo GM, Bordón JDR, Aznárez JJ. On the application of the beam model for linear dynamic analysis of pile and suction caisson foundations for offshore wind turbines. Comput Geotech 2021;134. http://dx.doi.org/10.1016/j.compgeo.2021.104107.

[34] Chen C, Duffour P, Fromme P. Modelling wind turbine tower-rotor interaction through an aerodynamic damping matrix. J Sound Vib 2020;489:115667. http://dx.doi.org/10.1016/j.jsv.2020.115667.
[35] Moll H-G, Vorpahl F, Busmann H-G. Dynamics of support structures for offshore wind turbines in fully-coupled simulations - influence of water added mass on jacket mode shapes, natural frequencies and loads. In: Proceedings of the European wind energy conference and exhibition, vol. 5, 2010, p. 3701–7, URL https://www.scopus.com/inward/record.uri?eid=2-s2.0-84870023107&partnerID=40&md5=76414d9bb1fcc695df2a31fd78a6660d,
[36] Bordón JDR, Álamo GM, Padrón LA, Aznárez JJ, Maeso O. Multifebe: A multi-domain finite element–boundary element solver for linear mixed-dimensional mechanical problems. SoftwareX 2022;20:101265. http://dx.doi.org/10.1016/j.softx.2022.101265.
[37] Domínguez J. Boundary elements in dynamics. WIT Press; 1993.
[38] Mantiĉ V. A new formula for the C-matrix in the somigliana identity. J Elasticity 1993;33:191–201. http://dx.doi.org/10.1007/BF00043247.
[39] Bak C, Zahle F, Bitsche R, Kim T, Yde A, Henriksen LC, Natarajan A, Hansen MH. Description of the DTU 10 MW reference wind turbine. DTU Wind Energy Report I-0092, Roskilde, Denmark: Technical University of Denmark; 2013.
[40] Eurocode. Eurocode 8: Design of structures for earthquake resistance. Part 5: Foundations, Retaining Structures and Geotechnical Aspects.. Brussels: European Committee for Standarization; 2004.
[41] Bond AJ, Hight DW, Jardine RJ. Design of piles in sand in the UK sector of the north sea. techreport OTH 94 457, Health & Safety Executive; 1997.
[42] Ohta Y, Goto N. Empirical shear wave velocity equations in terms of characteristic soil indexes. Earthq Eng Struct Dyn 1978;6(2):167–87. http://dx.doi.org/10.1002/eqe.4290060205.
[43] Kaynia AM. Effect of kinematic interaction on seismic response of offshore wind turbines on monopiles. Earthq Eng Struct Dyn 2021;50(3):777–90. http://dx.doi.org/10.1002/eqe.3371.
[44] Sandal K, Latini C, Zania V, Stolpe M. Integrated optimal design of jackets and foundations. Mar Struct 2018;61:398–418. http://dx.doi.org/10.1016/j.marstruc.2018.06.012.
[45] Novak M, Sharnouby BE. Stiffness constants of single piles. J Geotech Eng 1983;109(7). http://dx.doi.org/10.1061/(ASCE)0733-9410(1983)109:7(961).
[46] Doherty JP, Houslby GT, Deeks AJ. Stiffness of flexible caisson foundations embedded in nonhomogeneous elastic soil. J Geotech Geoenvironmental Eng 2005;131(12):1498–508. http://dx.doi.org/10.1061/(ASCE)1090-0241(2005)131:12(1498).
[47] Gazetas G. Foundation vibrations. In: Fang H-Y, editor. Foundation engineering handbook. second ed.. New York, NY: Van Nostrand Reinhold; 1991, p. 553–93. http://dx.doi.org/10.1007/978-1-4615-3928-5_15.
[48] Bordón JDR, Aznárez JJ, Padrón LA, Maeso O, Bhattacharya S. Closed-form stiffnesses of multi-bucket foundations for OWT including group effect correction factors. Mar Struct 2019;65:326–42. http://dx.doi.org/10.1016/j.marstruc.2019.01.008.
[49] Bhattacharya S, Nikitas N, Garnsey J, Alexander NA, Cox J, Lombardi D, Wood DM, Nash DFT. Observed dynamic soil–structure interaction in scale testing of offshore wind turbine foundations. Soil Dyn Earthq Eng 2013;54:47–60. http://dx.doi.org/10.1016/j.soildyn.2013.07.012.
[50] DNV AS. DNV: Guidelines for design of wind turbines. 2002, Ed. DNV/Riso.
[51] Yan Y, Yang Y, Bashir M, Li C, Wang J. Dynamic analysis of 10MW offshore wind turbines with different support structures subjected to earthquake loadings. Renew Energy 2022;193:758–77. http://dx.doi.org/10.1016/j.renene.2022.05.045, URL https://www.sciencedirect.com/science/article/pii/S0960148122006863.